Statistical Analysis of the Human Cardiac Fiber Architecture from DT-MRI

Herve Lombaert[1,2], Jean-Marc Peyrat[3], Pierre Croisille[4], Stanislas Rapacchi[4], Laurent Fanton[5], Patrick Clarysse[4], Herve Delingette[2], and Nicholas Ayache[2]

[1] École Polytechnique de Montréal, Canada
[2] Asclepios, INRIA Sophia-Antipolis, France
[3] Siemens Molecular Imaging, Oxford, UK
[4] CREATIS, Université de Lyon, France
[5] Institut Universitaire de Médecine Légale, Université de Lyon, France

Abstract. A statistical atlas of the cardiac fiber architecture is built for the first time with a human dataset of 10 healthy *ex vivo* hearts acquired using DT-MRI. The atlas is constructed using an efficient semi-automated method where limited interactions are only required to segment the myocardium. All hearts are registered automatically by an efficient and robust non linear registration method. The statistical atlas gives a better understanding of the human cardiac fiber architecture. The study on the global variability of the human cardiac fiber architecture reveals that the fiber orientation is more stable than the laminar sheet orientation. The variability is also consistent across the left ventricular AHA segments. Moreover this atlas could be used for cardiac electromechanical modeling as well as a basis for more precise extrapolation models, essential for *in vivo* cardiac DT-MRI acquisition.

1 Introduction

The beating heart undergoes complex deformations, and the study of the cardiac fiber architecture gives an opportunity to better understand these dynamics. Early studies relied on fiber dissections and histological slices [12]. Nowadays, with advances in imaging technologies, the cardiac fibers can be imaged via diffusion tensor magnetic resonance imaging (DT-MRI) [3,10]. Various acquisition schemes have been proposed for *in vivo* diffusion weighted imaging (DWI) [5,7]. However, due to the fast cardiac motion, its application is currently limited to single DT-MRI slices (2D). The full 3D *in vivo* imaging of the cardiac architecture should still rely on an extrapolation model [17] in the near future. Localized and direct *in vivo* measurements with a dedicated catheter is also possible [11], but is limited to sparse locations on the endocardial surface. The availability of a full 3D atlas of the cardiac architecture opens the door to not only the construction of more accurate extrapolation models for *in vivo* acquisitions, but also to a better understanding of various cardiac mechanical functions, cardiac electrophysiology patterns, and remodeling processes. So far only *ex vivo* canine DT-MRI studies [9,13] have been considered, and in humans, only cases using a single *ex vivo* heart has been studied [15] and visualized in 3D [16]. Histological and DT-MRI studies all lead to similar findings. The fibers, locally organised as laminar sheets, appear to be consistently

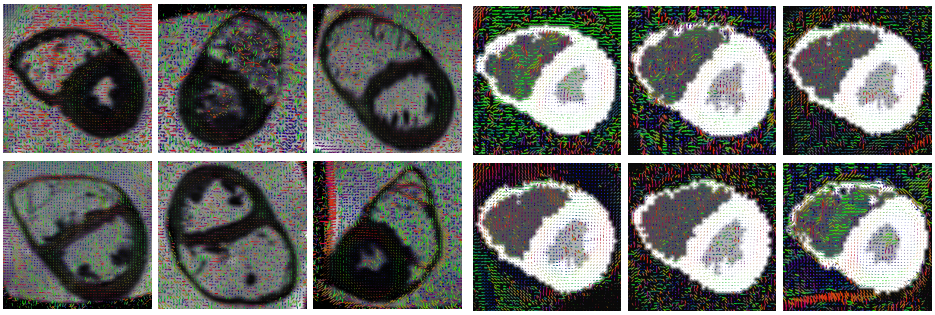

(a) Original tensor fields overlaid by the B_0 images

(b) Segmented B_0 images and registered tensor fields

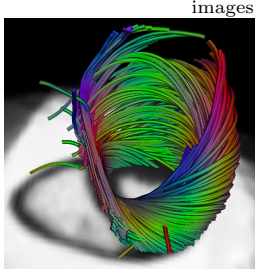

(c) Fiber tractography of the left ventricle and a short axis slice

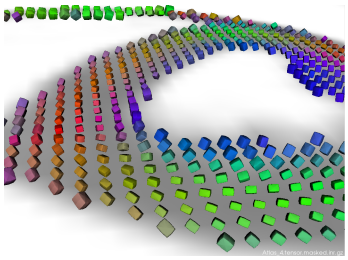

(d) Close up on the fiber orientations of a short axis slice

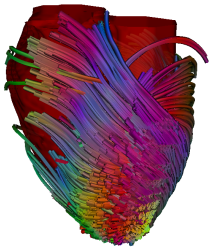

(e) Fiber tractography around the left ventricular blood pool

Fig. 1. A *statistical atlas* of the human cardiac fiber architecture is constructed from *(a)* 10 *ex vivo* human hearts (only 6 of them are shown). *(b)* They are segmented and registered to an average heart shape. The transmural variation of the fiber orientations in the left ventricle is visible in the fiber tractography (computed with MedINRIA) of the average tensor field. *(c)* It is overlaid with a short axis slice (with a close up view on *(d)*). *(e)* A long axis view of the left ventricle with the blood pool in red. The fiber coloring is dependent on the fiber orientation.

structured as two counter wound spirals where the fibers smoothly change orientation from the endocardium to the epicardium. Their orientation seems to be more stable than the laminar sheet orientation [9,13].

The availability of human hearts is extremely difficult (they are rather transplanted than used for research), and thanks to a unique post-mortem human dataset [6,14], we have built a statistical atlas from *ex vivo* DT-MRI and extended previous studies [9,13] to humans. The next section explains the semi-automatic method used to construct such atlas. The last section provides global statistics on the fiber architecture as well as more local properties within several myocardial segments.

2 Materials and Method

A method requiring the least possible interactions has been developed. The user provides two paint strokes in a B_0 image, one in each ventricle, and the method finds automatically the myocardium, registers it to the other myocardia, and constructs the statistical atlas of the fiber architecture. The construction of the atlas requires thus minimal user interaction, is reproducible, and can be quickly ex-

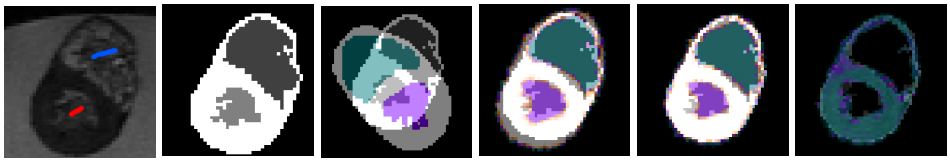

(a) Painted strokes (b) Labeled image (c) Alignment of ventricles (d) Rigid registration (e) Non-rigid registration (f) with masked images

Fig. 2. *Segmentation*: (a) The user marks the left and right blood pools on B_0 images (red and blue strokes), (b) a segmented image is created via Graph Cuts. *Registration*: The method (c) aligns the ventricles of the segmented images, (d) performs a rigid registration, and finds the non-rigid registration between (e) the segmented and (f) the masked B_0 images.

tended with additional hearts. From this atlas, the fiber variability is analyzed using state-of-the-art statistical tools on diffusion tensors within an efficient Log-Euclidean framework.

2.1 Data acquisition

The human dataset [6,14] consists of 10 *ex vivo* human hearts acquired during forensic autopsies (6 of them are presented in Fig. 1(a)). MR imaging was performed within 24 hours after death, prior to the examination of the heart and lungs by the pathologist. All cases were from extra cardiac sudden deaths, and hearts were classified as healthy after controlling their weight, wall thickness, and subsequent pathology examination. The excised hearts were placed in a plastic container and filled with hydrophilic gel to maintain a diastolic shape. All images have been acquired on a 1.5T MR scanner (Avanto Siemens) with a bipolar echo planar imaging using 4 repetitions of 12 gradient images. The volumes are of size 128x128x52 with an isotropic resolution of 2mm. Each tensor image is globally normalized by aligning the histograms of the traces of the tensor matrices to compensate for any acquisition variability. This normalization does not affect the orientations of the eigenvectors.

2.2 Segmentation

The myocardium segmentation is a crucial part in our atlas construction, and the Graph Cut algorithm [4] has been chosen for its efficiency and ease of use. From a B_0 image, an underlying 3D graph is constructed and a global optimal solution partitions the graph into an *object* and a *background*. Fast interactions are possible to correct any missed segmentation. In our application, the user marks on a 3D slice a few pixels, the *seeds* ([4]), in the left and right blood pools (red and blue strokes in Fig. 2 (a)). From these marks, three 3D binary segmentations are performed: *i)* the heart is isolated from its background using the marked pixels as *object seeds* [4] and the pixels lying on a surrounding box (large enough to be outside the heart) as *background seeds*, *ii)* the myocardium is delineated using the pixels on the inner boundary of the heart mask as *object seeds* and the marked pixels as *background seeds*, and *iii)* the blood pool is partitioned into the left and right sides using each paint stroke as *seeds*. From these binary masks, a 3D segmentation image is created with four labels: background, left and right ventricles, and myocardium (Fig. 2(b)).

2.3 Registration and atlas construction

To construct the atlas of DT-MRIs, the population of hearts must be registered to a common reference heart shape. The registration is solely based on B_0 images and their segmented images. Information on the fiber architecture are purposely omitted in order to avoid any bias in the study of the fiber variability. After aligning the centers of mass of each ventricle (Fig. 2(c)), a block matching algorithm performs a rigid registration on the segmented images (Fig. 2(d)). Once correctly aligned, a non-rigid registration of the segmented images is performed (Fig. 2(e)). The resulting transformation initializes the registration of the masked B_0 images (Fig. 2(f)). The symmetric log-domain diffeomorphic demons [18] provides an efficient non-rigid registration method. Moreover, averaging and inverting diffeomorphic deformation fields are straightforward in the log-domain. The construction of the atlas follows Guimond's *et al.* method [8], where the average of inverse transforms brings iteratively the reference heart toward an average shape. In practice, the reference image becomes stable after two or three iterations. Finally, the tensor fields associated with each B_0 image are warped to the converged average heart shape. Among two possible reorientation strategies [1], the Finite Strain strategy is preferred to the Preservation of the Principal Direction for its preservation of geometric features [13].

2.4 Statistical analysis

A voxel-wise statistical analysis is performed on our atlas (i.e., a population of diffusion tensors warped to a reference heart). The Log-Euclidean metric [2] provides a fast and valid framework for the study of the variability of the diffusion tensors. Our study uses classical statistical tools (such as the mean or the covariance) in the Log-Euclidean framework rather than in the Euclidean space. A tensor is described with a condensed form, $\mathrm{vec}(D) = (D_{11}, \sqrt{2}D_{12}, D_{22}, \sqrt{2}D_{31}, \sqrt{2}D_{32}, D_{33})^t$, where redundant terms in the tensor matrix $(D_{ij})_{i,j=1,2,3}$ are removed. With N tensor fields, $\{D^{(i)}\}_{i=1,\ldots,N}$, the mean is computed, $\bar{D} = \exp\left(\frac{1}{N}\sum_{i=1}^{N}\log(D^{(i)})\right)$, along the covariance matrix, $\Sigma = \frac{1}{N-1}\sum_{i=1}^{N}\mathrm{vec}(\Delta D^{(i)})\cdot\mathrm{vec}(\Delta D^{(i)})^t$ where $\Delta D^{(i)} = \log(D^{(i)}) - \log(\bar{D})$. The trace of the covariance matrix (i.e., the sum of its eigenvalues) gives an assessment on the global variability of the tensor field. To express it as a percentage ratio from the mean tensor $\bar{D}$, we use its square root:

$$\sqrt{\mathrm{Tr}(\Sigma)} = \sqrt{\frac{1}{N-1}\sum_{i=1}^{N}\|\mathrm{vec}(\Delta D^{(i)})\|}. \tag{1}$$

To gain further information on the variability of the tensor field, The covariance matrix is projected onto orthonormal bases [13]. These bases are formed with a combinations of the different eigenvectors $\mathbf{v_1}, \mathbf{v_2}, \mathbf{v_3}$ of the mean tensor matrix $\bar{D}$. The bases of particular interest are $W_{2,3} = 1/\sqrt{2}\,(\mathbf{v_3}\cdot\mathbf{v_2}^t + \mathbf{v_2}\cdot\mathbf{v_3}^t)$, $W_{1,3} = 1/\sqrt{2}\,(\mathbf{v_3}\cdot\mathbf{v_1}^t + \mathbf{v_1}\cdot\mathbf{v_3}^t)$, and $W_{1,2} = 1/\sqrt{2}\,(\mathbf{v_2}\cdot\mathbf{v_1}^t + \mathbf{v_1}\cdot\mathbf{v_2}^t)$. The standard deviation of orientation differences, $\{\theta_{i,j}\}_{i,j=1,2,3}$, between the coupled $(\mathbf{v_i}, \mathbf{v_j})$ axes around $\mathbf{v_k}$ (i.e., the variability of how the orthogonal axes $(\mathbf{v_i}, \mathbf{v_j})$ rotates

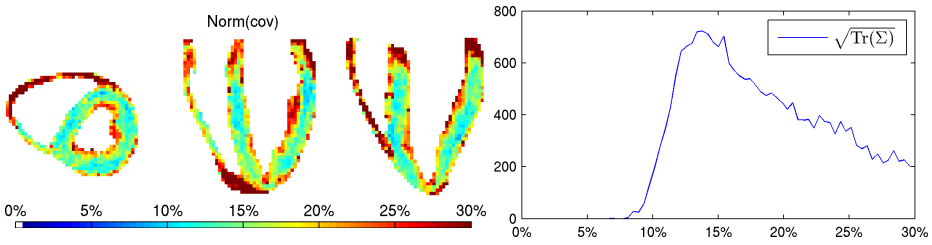

Fig. 3. Global variability ($\sqrt{\mathrm{Tr}(\Sigma)}$, Eq. 1) (expressed in percentage) of the human cardiac fiber structure. The histogram shows a mode of 13.2%.

around $\mathbf{v_k}$) are revealed by projecting the covariance matrix Σ onto $W_{2,3}$, $W_{1,3}$, and $W_{1,2}$ ($\lambda_{1,2,3}$ are the tensor eigenvalues):

$$\theta_{i,j} = \arctan\left(\frac{1}{2(\lambda_i - \lambda_j)^2}[\mathrm{vec}(W_{i,j})^t \cdot \Sigma \cdot \mathrm{vec}(W_{i,j})]\right)^{\frac{1}{2}} \tag{2}$$

3 Results

The variability of the global fiber architecture is first presented, followed by a more local study on the 17 AHA (American Heart Association) cardiac zones in the left ventricle.

3.1 Fiber variability

The tractography of the cardiac fibers in Figure 1 shows the average fiber structure. The transmural variation of the fiber orientation is clearly seen in all views. The fibers form a double spiral with different orientations on each side of the myocardium mid-wall. The histogram of the trace (Fig. 3 using Eq. 1) shows a peak of variability at 13.2%. It is however important to note that this variability also includes registration errors. The registration can be difficult and challenging (large deformations, low resolutions) and could certainly be the cause of a higher variability in the right ventricle, the papillary muscles, and around the apex. The variability of the eigenvectors (Fig. 4) reveals a disparity among the different directions. Indeed, the rotations of the planes containing the first eigenvector (i.e., the fiber orientation) around perpendicular axes $\mathbf{v_2}$ and $\mathbf{v_3}$ ($\theta_{1,3}$ and $\theta_{1,2}$ using Eq. 2) show a rather stable cardiac fiber orientation with a standard deviation of $\theta_{1,3} = 11.5°$and $\theta_{1,2} = 13.0°$. However, the orientation of the coupled axes $(\mathbf{v_2}, \mathbf{v_3})$ (i.e., the laminar sheets) around the fiber orientation $\mathbf{v_1}$ shows a much greater variability in the laminar sheet structure with $\theta_{2,3} = 31.1°$. This concurs with a previous canine study [13] where the fiber orientation (with $\theta_{1,3} = 7.9°$and $\theta_{1,2} = 7.7°$) is more stable than the laminar sheet orientation (with $\theta_{2,3} = 22.7°$).

3.2 Variability across myocardial segments

We register and map the statistical atlas onto a prolate ellipsoid, and analyze the transmural variation of the fiber orientation in the 17 AHA segments of the left ventricle. The figure 5 shows the helix angle (between the fiber orientation and

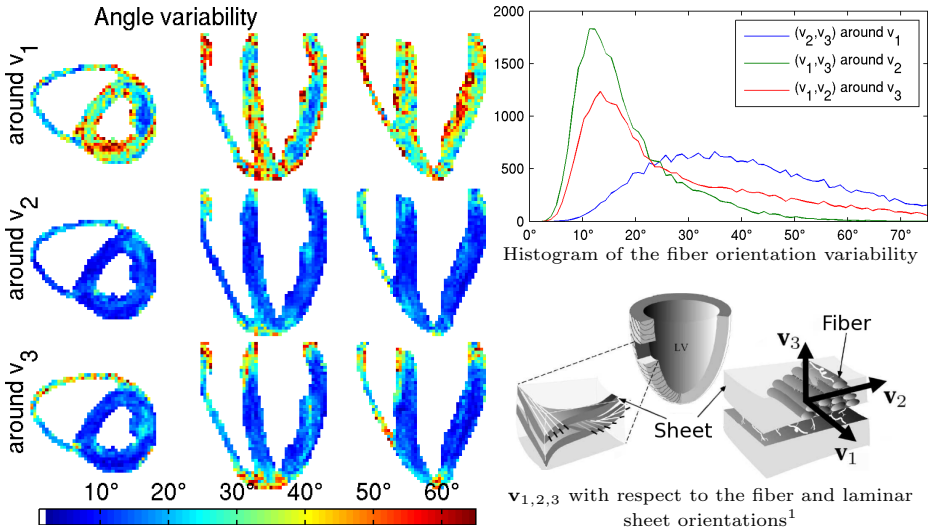

Fig. 4. Standard deviation of the fiber orientation (expressed in degree). *Top row of the image and in the blue histogram*: Variability of the laminar sheet orientation, $\theta_{2,3}$ around $\mathbf{v}_1$, with a mode at 31.1°. *Middle row and in the green histogram*: Variability of the fiber orientation, $\theta_{1,3}$ around $\mathbf{v}_2$, with a mode at 11.5°. *Bottom row and in the red histogram*: Variability of the fiber orientation, $\theta_{1,2}$ around $\mathbf{v}_3$, with a mode at 13.0°.

a short axial line) and the transverse angle (between the fiber orientation and a long axial line) against the transmural width. The helix angle varies globally from -51°on the epicardium to +66°on the endocardium (the range is 117°- a canine study [13] showed a range of 110°). It appears to be consistent across all myocardial segments. There is however a drastic difference at the apex. While this might be due to missed registrations in the apex area, this could also mean that the fiber structure at the apex varies among the human population. The helix angle is strongly correlated to the transmural distance with a correlation factor of $\rho = 0.831$. The transverse angle is less correlated with $\rho = 0.286$ (i.e., it depends less on the transmural width). It is stable at 0°and appears to be always close to zero on all myocardial segments.

4 Conclusion

This paper brings the first statistical description of the human cardiac fiber architecture from 10 *ex vivo* DT-MRI images. The statistical atlas has been built thanks to a unique access to 10 *ex vivo* human hearts. The fiber variability has been studied across the whole myocardium. The results show that the orientations of the cardiac fibers are more stable than the cardiac laminar sheet orientations. Knowing that the fibers are globally stable, it was interesting to study the fiber orientation in a more local manner in the left ventricular AHA zones. The observed orientation is consistent across nearly all myocardial segments. Only the apex shows a higher variability. This might show that the fiber structure at the

[1] Illustration adapted from LeGrice *et al.*, *Am. J. of Phys. - Heart and Circ. Phys.*, 269(2), 1995.

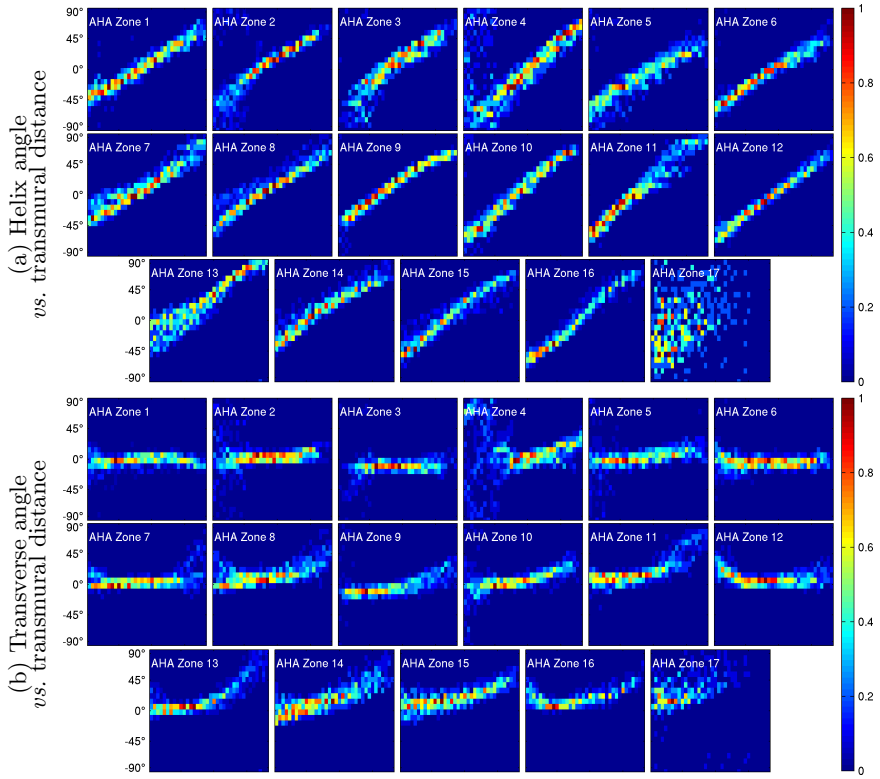

Fig. 5. Joint histograms showing the distribution of the *(a)* helix angle and the *(b)* transverse angle of the human cardiac fibers across the myocardial wall in the 17 AHA segments of the left ventricle. The x axis of each joint histogram represents the transmural distance from epicardium *(left)* to endocardium *(right)*. The y axis is the helix or transverse angle.

apex might not have a consistent structure. The results of this study also extend a previous canine study [13]. Moreover, a semi-automatic method has been described to build a morphological atlas with easy user interactions. It can be reused for other future studies using more samples or other species. The fiber architecture plays a key role in mechanical and electrical cardiac functions. This first statistical atlas of the human cardiac fiber architecture allows thus a better understanding of the human heart. With recent advances in *in vivo* DT-MRI, it is possible to foresee the use of this statistical model of the heart to extrapolate sparse *in vivo* acquisitions and thereupon paving the way for personalized *in vivo* DT-MRI.

Acknowledgement

The authors wish to thank the financial support of the National Science and Environment Research Council (NSERC), the Michael Smith Scholarship (CGS-MSFSS), and the EGIDE/INRIA Scholarship.

References

1. Alexander, D. C., Pierpaoli, C., Basser, P. J., and Gee, J. C. Spatial transformations of diffusion tensor magnetic resonance images. *IEEE Trans. on Medical Imaging*, 20(11), 2001. 4
2. Arsigny, V., Fillard, P., Pennec, X., and Ayache, N. Log-Euclidean metrics for fast and simple calculus on diffusion tensors. *Mag. Res. in Med.*, 56(2), 2006. 4
3. Basser, P. J., Mattiello, J., and LeBihan, D. MR diffusion tensor spectroscopy and imaging. *Biophysics Journal*, 66(1), 1994. 1
4. Boykov, Y. and Jolly, M.-P. Interactive organ segmentation using graph cuts. In *MICCAI*, 2000. 3
5. Dou, J., Tseng, W.-Y. I., Reese, T. G., and Wedeen, V. J. Combined diffusion and strain MRI reveals structure and function of human myocardial laminar sheets in vivo. *Mag. Res. in Med.*, 50(1), 2003. 1
6. Frindel, C., Robini, M., Croisille, P., and Zhu, Y.-M. M. Comparison of regularization methods for human cardiac diffusion tensor MRI. *Med. Im. An.*, 13(3), 2009. 2, 3
7. Gamper, U., Boesiger, P., and Kozerke, S. Diffusion imaging of the in vivo heart using spin echoes–considerations on bulk motion sensitivity. *Mag. Res. in Med.*, 57(2), 2007. 1
8. Guimond, A., Meunier, J., and Thirion, J. P. Average Brain Models: A Convergence Study. *Comp. Vis. and Im. Und.*, 2000. 4
9. Helm, P. A., Tseng, H.-J. J., Younes, L., McVeigh, E. R., and Winslow, R. L. Ex vivo 3D diffusion tensor imaging and quantification of cardiac laminar structure. *Mag. Res. in Med.*, 54(4), 2005. 1, 2
10. Hsu, E. W. and Henriquez, C. S. Myocardial fiber orientation mapping using reduced encoding diffusion tensor imaging. *J. of Card. Mag. Res.*, 3(4), 2001. 1
11. Lasher, R. A., Hitchcock, R. W., and Sachse, F. B. Towards modeling of cardiac micro-structure with catheter-based confocal microscopy: a novel approach for dye delivery and tissue characterization. *IEEE Trans. on Medical Imaging*, 28(8), 2009. 1
12. Nielsen, P. M., Le Grice, I. J., Smaill, B. H., and Hunter, P. J. Mathematical model of geometry and fibrous structure of the heart. *Am. J. of Phys. - Heart and Circ. Phys.*, 260(4), 1991. 1
13. Peyrat, J.-M., Sermesant, M., Pennec, X., Delingette, H., Xu, C., McVeigh, E. R., and Ayache, N. A Computational Framework for the Statistical Analysis of Cardiac Diffusion Tensors: Application to a Small Database of Canine Hearts. *IEEE Trans. on Medical Imaging*, 26(11), 2007. 1, 2, 4, 5, 6, 7
14. Rapacchi, S., Croisille, P., Pai, V., Grenier, D., Viallon, M., Kellman, P., Mewton, N., and Wen, H. Reducing motion sensitivity in free breathing DWI of the heart with localized Principal Component Analysis. In *ISMRM*, 2010. 2, 3
15. Rohmer, D., Sitek, A., and Gullberg, G. T. Reconstruction and visualization of fiber and laminar structure in the normal human heart from ex vivo diffusion tensor magnetic resonance imaging (DTMRI) data. *Investigative Radiology*, 42(11), 2007. 1
16. G. Seemann, D. U. J. Keller, D. L. Weiss, and O. Dossel. Modeling human ventricular geometry and fiber orientation based on diffusion tensor MRI. In *Comp. in Card.*, 2006. 1
17. Toussaint, N., Sermesant, M., Stoeck, C. T., Kozerke, S., and Batchelor, P. G. In vivo human 3D cardiac fibre architecture: reconstruction using curvilinear interpolation of diffusion tensor images. In *MICCAI*, 2010. 1
18. Vercauteren, T., Pennec, X., Perchant, A., and Ayache, N. Symmetric log-domain diffeomorphic registration: A demons-based approach. In *MICCAI*. 2008. 4